An experimental study of a flow-accelerating hydrokinetic device

Brian Mannion*[1], Vincent McCormack[2], Ciaran Kennedy[1], Seán B. Leen[1] & Stephen Nash*[1]

[1]*College of Engineering & Informatics, National University of Ireland, Galway, Ireland and SFI Centre for Marine Renewable Energy Ireland.*
[2] *GKinetic Energy LTD, Limerick, Ireland.*

*b.mannion4@nuigalway.ie
*stephen.nash@nuigalway.ie

Abstract

Tidal energy researchers and developers use experimental testing of scaled devices as a method of evaluating device performance. Much of the focus to date has been on horizontal axis turbines. This study is focused on a novel vertical axis turbine which incorporates variable-pitch blades and a flow accelerator. The research involves laboratory testing of scale model devices in a recirculating flume. Computational fluid dynamic modelling is used to reproduce the measured flow data to investigate disparities in experimental data. The results show that the device is capable of achieving localised flow acceleration of up to a factor of 2 above the freestream velocity and achieved a mechanical power efficiency of 40%.

Keywords: Tidal turbine; Vertical axis; Flow acceleration; Variable-pitch; Power coefficient

Nomenclature

Symbol	SI unit	Definition
U_∞	m/s	Ambient velocity
μ	kg/m s	Viscosity
A, A_c	m^2	Area
ADCP		Acoustic Doppler current profiler
CFD		Computational fluid dynamics
C_D		Drag coefficient
C_L		Lift coefficient
C_P		Power coefficient/coefficient of performance
D_b	m	Bluff body diameter
L	m	Length
F_{Drag}	N	Drag force
P_{avail}	W	Available Power
P_{mech}	W	Mechanical Power
R	m	Radius
R_e		Reynolds number
T	Nm	Torque
TSR, λ		Tip speed ratio
α, *AOA*	deg	Angle of attack
ρ	kg/m^3	Density
VATT		Vertical axis tidal turbine
ω	rad/s	Rotational velocity

1 Introduction

Tidal stream energy is an attractive source of renewable energy. Due to the fact that tides are controlled by the lunar and solar cycles, tidal energy availability is much more predictable than other renewable sources such as wind, wave and solar. The tidal stream energy sector is still at an early stage of development with very few utility-scale energy converters deployed to date. The majority of tidal stream converters fall into one of two categories - horizontal axis turbines or vertical axis turbines. For both types, the tidal current generates lift and drag forces on the turbine rotor causing it to turn about the device's horizontal or vertical axes, generating mechanical power. Most devices are predominantly lift-based, as drag type turbines such as the Savonius, have a low efficiency[1]. Many devices are still at early stages of research and development, but a number of devices, primarily horizontal axis turbine designs, are at an advanced stage of development. For example, the Marine Current Turbine (MCT), is a 1.2 MW, horizontal axis, twin turbine ("SeaGen") operating in Strangford Lough, Northern Ireland since 2008, with a demonstrated peak mechanical efficiency of 48 % [2]. Verdant Power's three-bladed horizontal axis turbine has also been deployed at full-scale and achieved a mechanical efficiency of 43 %[3]. Other market leaders include Andritz Hydro Hammerfest[4], Atlantis[5], Scotrenewables[6], Voith[6] and OpenHydro[7], all of which are of the horizontal axis turbine design.

The turbine which is the focus of this research is a vertical axis design. Figure 1 shows a computer-generated image of the device and a picture of a 1:10 scale model during field tests. The device comprises two high solidity 'squirrel cage' vertical axis rotors on either side of a central *bluff body* and has two unique design features. First, the bluff body acts to accelerate the entrance flows to the turbines above freestream levels and, second, the pitch of the turbine blades is controlled so as to maximise the turbine torque. The blade pitching mechanism comprises a patented cam track which controls the pitch of the blades. The design of the cam track was informed by computational fluid dynamics (CFD) analysis which determined the optimum angle of attack, and thus the pitch angle for each azimuthal position of the blade, for chosen maximum torque. The turbines consist of six NACA 0018 profile blades. At a specific position in the turbine's rotation cycle, the blades undergo a 70° change in pitch and the symmetrical profile ensures that both sides of the blade exhibit the same lift and drag characteristics. The turbine rotors are positioned at the widest points of the bluff body to coincide with the points of maximum flow acceleration as determined from the scale model studies presented here. The device is designed to float in the water column such that the turbines are fully submerged and is moored to the seabed. The bluff body also acts as a ballast tank, with water added or removed during deployment and retrieval.

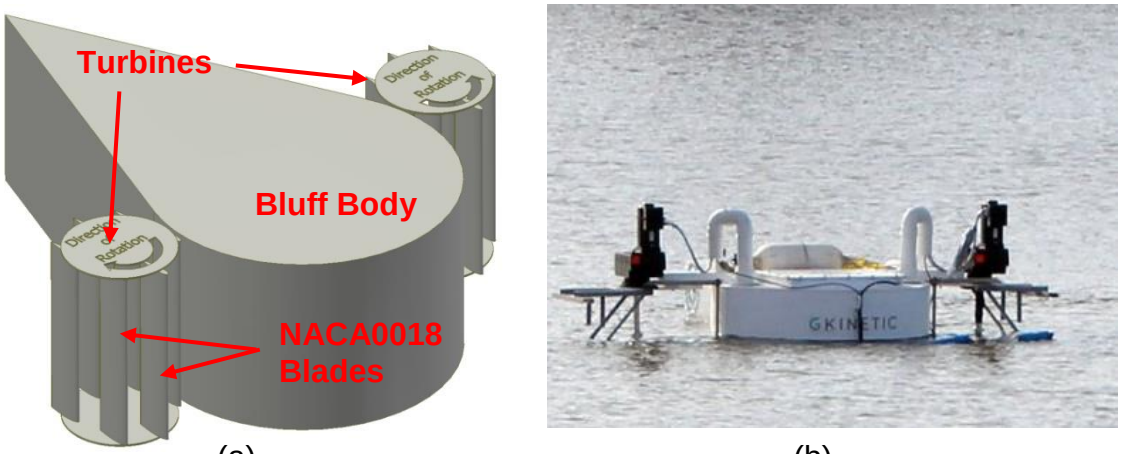

Figure 1. (a) Solid model of the GKinetic tidal turbine; (b) photograph of deployed device.

The flow acceleration concept was motivated by the cube relationship between power available in a moving stream and fluid velocity. The majority of leading tidal turbines are only economically viable in water with peak current speeds of at least 2 m/s. Globally, such high energy flows are rare. The flow acceleration incorporated in the present device means that it can be deployed in areas of lower tidal speeds. Roddier et al.[8]showed the potential for accelerating current velocities in regions where tidal flows are not sufficiently energetic for extraction to be feasible. The latter examined the possibility of using a large structure (i.e. a bluff body) to cause an acceleration of local current velocities onto an underwater disc. A flume study was performed to measure the force on the disc, with and without the accelerating structure, and it was determined that the force was 50 % higher with the accelerator in place. Flow accelerates around obstacles and the work of Gerrard[9] showed that the inclusion of a splitter plate can weaken vortex strength and decrease vortex frequency downstream. Graf and Yulistiyanto[10] studied flow around cylinders in a tilting flume and noted maximum localised accelerations of depth-averaged flow speeds of 100 % at the widest point of the cylinder. The flow acceleration concept was tested for the present device using a 1:40 scale model of the bluff body.

The power coefficient (C_P) of a tidal turbine measures the efficiency with which it converts available tidal stream power into usable power and can be quoted relative to either mechanical or electrical power. The theoretical upper limit of C_P is 0.59, known as the Betz limit, but actual C_P values will be lower due to energy losses during the conversion process. The leading technologies have achieved mechanical C_P values in the region of 0.4 to 0.5 (or 40 % to 50 % efficiency). With regard to scale model testing of tidal turbines, O'Doherty et al.[11] tested a horizontal axis turbine using a recirculating flume and determined an average C_P of 0.41, while Clarke et al.[12] conducted a similar study of a horizontal axis turbine in a towing tank and recorded a peak C_P of 0.39. Goundar & Ahmed[13] used an experimentally validated CFD model in order to predict the performance of a three-bladed horizontal axis turbine and documented a C_P of 0.47. With regards to vertical axis turbines, which are of more relevance to this research, Bachant and Wosnik[14] performed tow testing on a three-bladed, fixed-pitched turbine and recorded C_P values ranging from 0.19 to 0.27 depending on the Reynolds number (based on turbine diameter). New Energy Corporation has developed fixed pitch devices comprising of both four and five blades that achieved a

C_P of 0.32[15]. Finally, Jing et al.[16] conducted tow tests of a turbine with six straight blades incorporating variable pitch control and achieved an average C_P of 0.25.
One of the novel features of the device tested here is the acceleration of the flow around the central bluff body before entering the turbines. The acceleration of inlet flows has been incorporated in other turbine designs using ducts (either internal or external) and has been shown to have positive effects on device performance. However, one must be careful when determining efficiencies for ducted turbines as (1) the Betz limit no longer applies[17] and (2) the duct area rather than the turbine area should be used as the device reference area[18]. However, the latter point is often ignored in the literature. Elbatran et al.[19] and Derakhshan et al.[20] both used CFD model studies to show how the inclusion of a nozzle/duct improved turbine performance by 78 % and 52 %, respectively, in comparison to a conventional turbine design but both studies used the smaller turbine area as the reference area. Jin et al.[21] also showed that by placing a deflector plate upstream of dual vertical axis turbines, turbine efficiency could be increased from 33 % to 42 %. Again though, the reference area was reported as the turbine swept area and did not account for the additional area of the deflector. In the present research, power coefficients (i.e. efficiencies) are calculated using the full device entrance area rather than just the turbine area.

This paper presents details of the experimental testing of a flow-accelerating vertical axis turbine at various scales. Flow acceleration was initially investigated by testing a scale model of the bluff body in a tidal basin. Subsequent testing of the device was conducted in a recirculating flume with the primary objective being the characterisation of device performance, particularly in relation to determining the mechanical efficiency of the device and the tip speed ratio at which the peak value occurs. An additional objective was to determine drag loads on the device. The methodology and instrumentation used for the scale model tests are described in Section 2 and the test results are presented in Section 3. CFD modelling of the accelerated flows produced by the turbine bluff body is presented and the results are compared with measured flow speeds from laboratory experiments. An indirect method of mechanical power measurement is also detailed. A peak mechanical C_P of 40 % was measured in a free-stream velocity of 1.1 m/s.

2 Methodology

To date, testing of the tidal stream device has progressed from 1:40 scale models (bluff body diameter of 0.4 m and turbine diameter 0.15 m) to 1:20 scale models (bluff body diameter of 1.64 m and turbine diameter 0.6 m). The scaling is based on the device entrance area. The concept of the flow accelerating bluff body was initially tested at 1:40 scale in the NUI Galway tidal basin and subsequently at 1:20 scale in the IFREMER wave-current recirculating flume in Boulogne-Sur-Mer, France. The flume is 18 m long, 4 m wide and 2.1 m deep; it is capable of producing flow speeds in the range 0.1 to 2.2 m/s. Device performance was determined during the 1:20 scale tank tests. Development of the testing methodologies relied on two guidance documents. “Best practice for tank testing of small marine energy devices” by McCombes et al.[22] contains extensive detail on the design of experiments and uncertainty analysis methodologies while the “Tidal current energy device development and evaluation protocol” by the University of Southampton[23] identifies five key milestones in the development of a commercial scale tidal energy extraction

device. The current device is at Stage 2 of this development scale which requires physical testing at an intermediate stage.

Table 1 summarises the tests that were conducted during the research, giving the freestream velocity ranges tested and the measured performance parameters.

Table 1. Variables measured for each scale model device.

Measured Variable	Free-stream Flow Speeds (m/s)	
	1:40 scale model	1:20 scale model
Flow around bluff body	0.3	0.8
Flow around device	0.8	0.8
Mechanical power	-	0.4 to 1.2
Drag loads	0.8 and 1	0.4 to 1.2

CFD modelling of the 1:20 scale bluff body was also conducted to investigate discrepancies between the flow acceleration measurements from the 1:40 and 1:20 scale tests. Model development studies showed that the Transition SST turbulence model was the turbulence model that most accurately reproduced the flow around the bluff body.

2.1 Experimental Testing

2.1.1 1:40 scale model

A 1:40 scale model consisting solely of the bluff body was initially tested in a tidal basin at NUI Galway to test the flow acceleration concept. An image of the test setup is shown in Figure 2a where the bluff body is located in the centre of the experimental area of the basin. The dimensions of the experimental area of the basin are 5 m x 4.75 m, with a maximum depth of 0.37 m. Using a Nortek Acoustic Doppler Velocimeter (ADV), current velocity measurements were taken along four radial transects at 0°, 45°, 90° and 135°. Figure 3b shows the circumferential positioning of transects in relation to the flow direction.

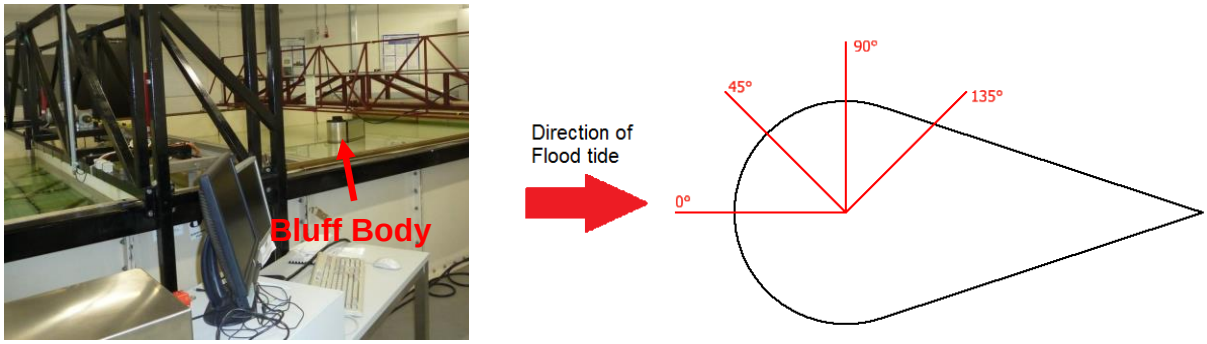

(a) (b)

Figure 2. (a) NUI Galway tidal basin. (b) ADV measurement Transect position.

Noise is an inherent property of any ADV and can be caused by a number of factors including the finite residence time for suspended particles in the sampling volume and small-scale turbulence (at scales similar to or less than the sampling volume). To minimise signal-to-noise ratio (SNR), a neutrally buoyant spherical seeding material of diameter 8 to 10 μm was dispersed within the water. In addition, based on the work of Dane[24], post-processing smoothing was applied to velocities via a first-order recursive filter of the form:

$$y_{\mathrm{i}} = \alpha_{\mathrm{filt}} y_{(\mathrm{i}-1)} + (1 - \alpha_{\mathrm{filt}})\mathrm{x}_{\mathrm{i}} \quad (1)$$

where x_{i} is the raw data value for sample number i; y_{i} is the mean of the local data values and α_{filt} is a smoothing parameter for low pass filter; $\alpha_{\mathrm{filt}} = (N_{\mathrm{filt}} - 1)/ N_{\mathrm{filt}}$ where N_{filt} is the total number of samples within the filter width.

All tests were run for the same tidal forcing condition, a repeating cyclic tide with amplitude 0.055 m and period 510 s. This resulted in high and low water levels in the working area of 0.2 m and 0.35 m. The tests were run for 6 tidal cycles with data averaged over the final four tidal cycles.

A second 1:40 scale model of the full device (bluff body and turbines) with rotating turbines (Figure 4) was tested in the IFREMER recirculating flume. The scale model was moored using the retention points on the floor of the flume and ballast was added to the bluff body until the device was brought to mid-depth. A single channel load cell was attached to the device allowing full device drag loads to be determined at this scale. The device was ballasted in order to improve its stability at the higher flow speeds. An LDV (Laser Doppler Velocimeter) was used to characterise the flow field around the device at a freestream flow speed of 0.8 m/s. LDVs use lasers to track the movement of microparticles (50 μm glass balls coated in silver) mixed in the water.

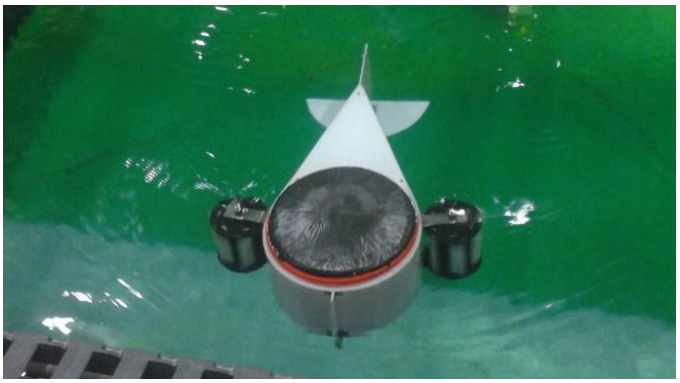

Figure 3. 1:40 scale device tested at IFREMER.

Mechanical power performance results were not determined for this scale device as implementing the blade pitching control system at such a small scale was not feasible; instead, the blades were allowed to rotate freely around their pivot points.

2.1.2 1:20 Scale Model

Due to dimensional constraints of the IFREMER test tank, it was only possible to test half of the complete device at 1:20 scale. This comprised a half-bluff body and a single turbine. Given that the device is symmetrical, this was deemed an acceptable

approach. A dimensioned plan view of the 1:20 scale model tested is shown in Figure 5(a), while an end elevation is presented in Figure 5(b). The turbine incorporates a blade pitching mechanism designed to enhance performance by ensuring that blade pitch is optimised throughout the revolution cycle. Figure 5 presents a graphical illustration of the pitching of each of the 6 blades at an instance in time. In this orientation the turbine rotates anticlockwise. It can be seen that the blade pitch changes as the blades turn along the upstream (front) end of the turbine; this is due to the gradients in velocity magnitude and direction as one moves outwards from the bluff body. There is also a noticeable difference in the pitch of the blades on the downstream side of the turbine compared to their upstream pitch positions. At blade position 3, the blade undergoes a pitch transition of about 70° where the angle of attack changes from a positive to a negative. This location was chosen for this large transition (or flip) so as to minimise the turbulence generated in doing so. The reason for the flip is because the blades were found to contribute more power from drag than lift when turning through the downstream portion of the cycle.

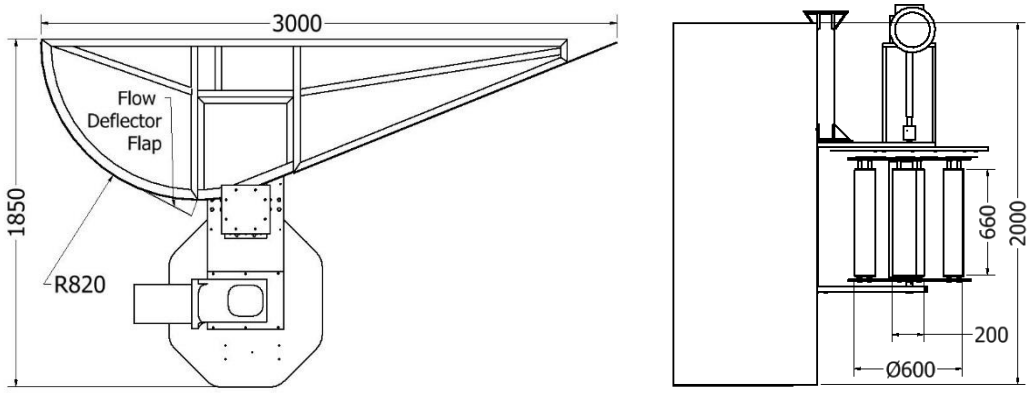

Figure 4. 1:20 scale device with outlining dimensions (mm); (a) plan view (b) end elevation.

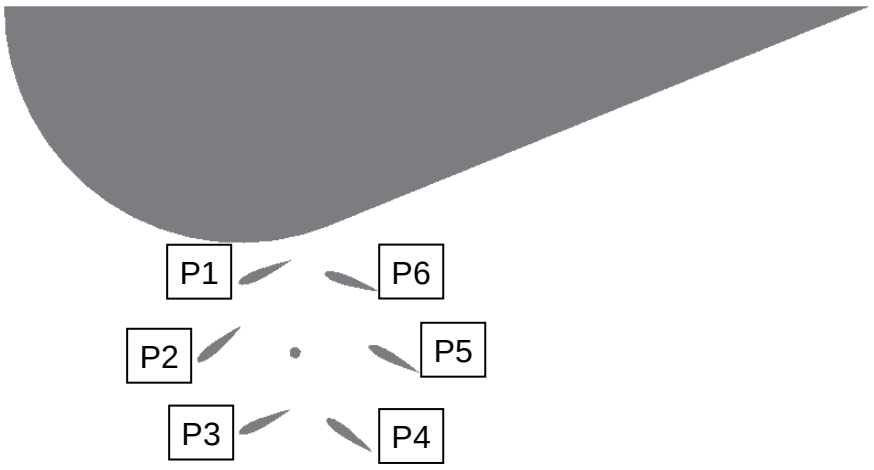

Figure 5. Schematic of turbine blade pitching relative to bluff body.

Flowfields were measured using the LDV, first around the bluff body alone at a flow speed of 0.8 m/s and subsequently with the turbine in position (Figure 6). The data for the bluff body alone was collected in order to determine the levels of flow acceleration achieved and make comparisons with the smaller scale tidal tank measurements.

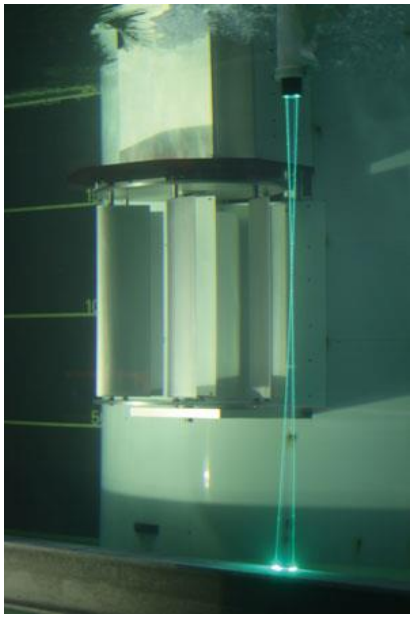

Figure 6. LDV characterising the bluff body flow for the tests at IFREMER.

In order to determine the mechanical power being produced, a torque meter was developed, consisting of four strain gauges configured in a full Wheatstone bridge and attached to the primary shaft of the turbine. The torque meter was connected to a Versalog BR model logger which recorded data at a frequency of 50 Hz. To convert strain to torque, the torque meter was calibrated. This involved restraining movement of the shaft in all directions at one end while applying a known torque via an incrementally increasing lever at the opposite end. Strain and torque data were graphed and a linear regression line was used to determine the relationship of strain to torque. Figure 7 shows the plotted data points which exhibited a perfectly linear relationship, allowing determination of a strain to torque conversion factor of 0.5961 Nm.

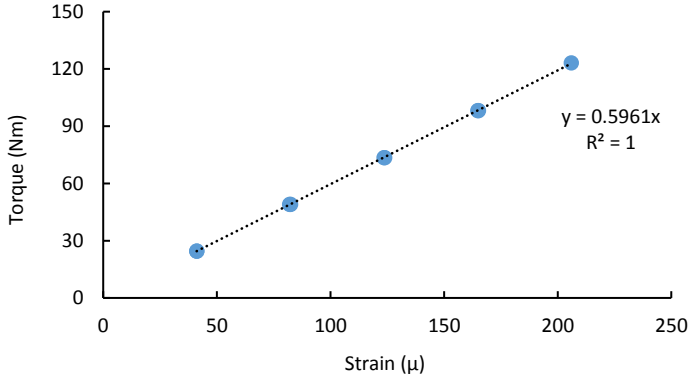

Figure 7. Torque meter calibration for strain to torque conversion.

During the 1:20 scale testing of the turbine, an Invertek variable speed drive was used to control the rotational speed of the turbine. This drive also logged the RPM value, which was validated by a tachometer. A speed increasing gearbox of ratio 73:1 was used. Induction motors have an inherent slippage flaw in their design, the magnitude

of which is a function of the air gap between the windings and the stator. This slippage causes a discrepancy between the full load speed and synchronous speed. However, Invertek's variable speed drive has a function known as "slip compensation" that allows the user to input the slippage value of the specific motor and the drive compensates for this slippage.

In order to determine the forces acting on the turbine, a load cell with six channels (three XYZ and three moments) was used. This apparatus was fixed between an arm on the turbine and the hexapod used to support it from overhead, allowing drag loadings on the turbine to be determined. The evaluation of these loads was important, as they inform the designing of the connections between the turbines and bluff body. The load-cell was set-up to record data at 100 Hz frequency intervals.

2.2 Relevant Equations

This section presents the equations that were used in determining the device performance parameters.

The total power available to the device in a free-stream flow with velocity U_∞ is:

$$P_{avail} = \frac{1}{2}\rho A {U_\infty}^3 \quad (2)$$

where ρ is the fluid density and A is the reference area (in this case, the frontal area of the half bluff body and turbine). The mechanical power of a rotating turbine is:

$$P_{mech} = T\omega \quad (3)$$

where T is torque and ω is the rotational velocity. The device performance coefficient, C_P, (otherwise known as the efficiency) is defined as:

$$C_P = \frac{P_{mech}}{P_{avail}} \quad (4)$$

The power coefficient varies with the tip speed ratio (λ), which is defined as the ratio of turbine rotational velocity to free-stream fluid velocity, expressed mathematically as:

$$\lambda = \frac{\omega R}{U_\infty} \quad (5)$$

where R is the turbine radius.

The drag force exerted on a body immersed in a moving fluid is:

$$F_{Drag} = \frac{1}{2}\rho {U_\infty}^2 A C_D \quad (6)$$

where C_D is the drag coefficient and A is again the reference area as defined in equation 2.

Finally, a fluid flow can be characterised using the Reynolds Number:

$$R_e = \frac{\rho U_\infty D}{\mu} \quad (7)$$

where μ is dynamic viscosity and D is either a device-related or flow-related length-scale.

Table 2 compares the Reynolds number values for the 1:20 and 1:40 scale model tests. The length scale taken is the diameter of the bluff body and the ambient flow speed is 0.8 m/s.

Table 2. Reynolds numbers of 1:20 and 1:40 scale devices.

Scale	R_e
1:20	1.3 x10^6
1:40	0.398 x10^6

Both Reynolds numbers determined are in the critical lower transition phase of the flow regime, allowing direct comparison of the model results. The comparison of Reynolds number values is based on previous work on cylinders[25]. Since the bluff body is basically a cylinder with a splitter attached this comparison is deemed acceptable.

2.3 Numerical Modelling

A 2D CFD model of the bluff body was developed in an effort to reproduce the flow accelerations measured in the experiments. Ansys Workbench version 17.1, and in particular Fluent, was used. An unstructured tri-element mesh was employed, with quad-element inflation layers used at the walls in order to accurately resolve the boundary layer. A first layer element height corresponding to a y^+ value of 1 was used in conjunction with the Transition SST turbulence model which was developed by Menter[26–28]. A total of 35 quad element layers was used, with a growth rate of 1.1. An image of the mesh which resulted in a mesh independent solution after a convergence study is shown in Figure 8. The entire mesh consisted of 398,000 elements in total with the highest concentration of elements around the bluff body. The mesh had a maximum skewness of 0.81.

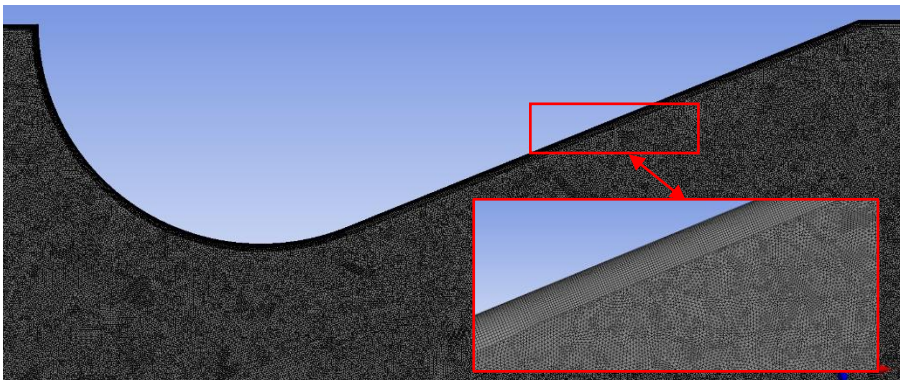

Figure 8. Mesh around bluff body with inset images showing the mesh close to the bluff body

In order to create the appropriate boundary layer effect within the model, *no-slip* shear conditions were applied to the tank walls and to the bluff body surface. The tank walls required appropriate wall roughness conditions and, in the absence of measured roughness values for the concrete walls of the IFREMER flume, a trial and error approach was used within a realistic value range for concrete (0.5 mm to 3 mm). The results from this model were compared to the flow speed measurements from the 1:20 scale model tests of the bluff body. The wall boundary conditions were then modified to remove the wall friction and symmetry boundary conditions were applied to the walls representing the tank; the model was re-run and the results were compared with those from the 1:40 scale model. The results from these models were used to investigate discrepancies between the two sets of measured flow data.

3 Results

The following section presents results from testing of two scale models of a vertical axis tidal energy device, as well as the results from the CFD modelling.

3.1 1:40 Scale Model Testing

In the tidal tank experiments of the 1:40 scale bluff body, current velocities were measured along four transects extending radially outwards from the centre of the bluff body at 0°, 45°, 90° and 135° to the incoming flow direction. For each transect, measurements were taken at five different distances from the wall of the bluff body: 80 mm, 120 mm, 160 mm, 200 mm and 240 mm. Figure 9 shows the velocities recorded along the transects at the mid-flood tide (i.e. the time of peak flood velocities) in the form of a vector plot. These data were averaged over four tidal cycles. The level of localised flow acceleration was determined by calculating the relative difference between the velocities recorded with and without the bluff body, i.e. the disturbed versus the undisturbed velocities.

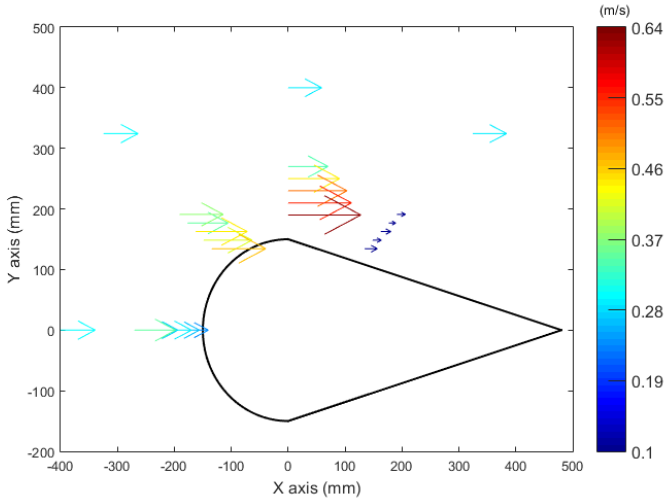

Figure 9. Current velocities recorded at the four transects for the 1:40 scale test in NUI Galway tidal basin.

Figure 9 clearly shows that the highest velocity increase occurs along the 90º transect, i.e. at the widest point of the bluff body, which agrees with the findings of previously published studies of flow around cylinders[9,29] and by studies carried out as part of this research, where similar results were observed for a cylinder of similar diameter. This was therefore identified as the optimum location for the turbines. The figure also shows that the accelerations are highest adjacent to the bluff body and that the flow speeds gradually returns to the freestream speed (0.3 m/s) away from the bluff body.

LDV results for the flow characterisation around the 1:40 scale device are presented in Figure 10. The turbines that were attached to the bluff body were less advanced than for the 1:20 scale model, e.g. there was no mechanism for controlling the pitching of the blades.

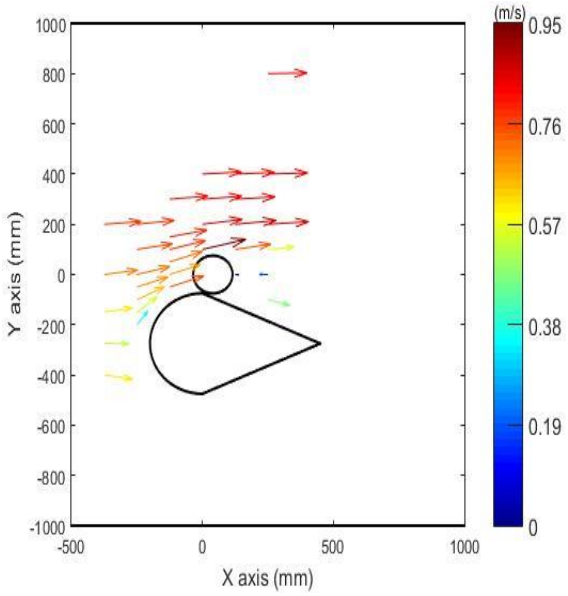

Figure 10. Vector plot of LDV data of 1:40 scale tests at IFREMER.

The forces measured on the 1:40 scale device were those exerted on the full device (a full bluff body and two turbines). The axial force component was taken as the drag force. Drag forces were averaged at ten-second intervals and are plotted in Figure 11 for freestream velocities of 0.8 and 1 m/s. Table 3 presents the average drag force calculated for each set of data from Figure 11. The overall averaged drag coefficient for this scale model is determined at 0.68.

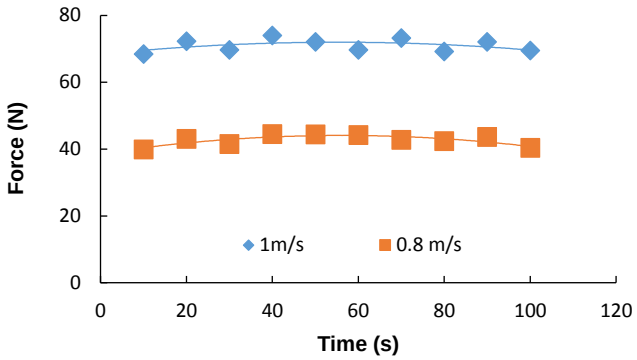

Figure 11. Effect of tidal velocity on measured drag force time histories for 1:40 scale device from IFREMER tests.

Table 3. Drag loads and drag coefficients of 1:40 scale device.

Flow Speed [m/s]	Drag Force (N)	C_D
0.8	42.94	0.66
1	70.95	0.70

3.2 1:20 Scale Model Testing

Flow measurements for the 1:20 scale device show the acceleration of velocity above the freestream level of 0.8 m/s by the bluff body. These results are presented in Figure 12 in the form of a vector plot. As in the 1:40 scale tidal basin tests, it is clear, that the increase in velocity is highest at the widest point of the bluff body. However, due to a frictional boundary layer that naturally occurs along a solid boundary, the magnitudes of acceleration are lower than in the tidal basin tests. The boundary layer was visually observed to be approximately half the width of the bluff body, nevertheless; an acceleration in excess of 60 % was recorded.

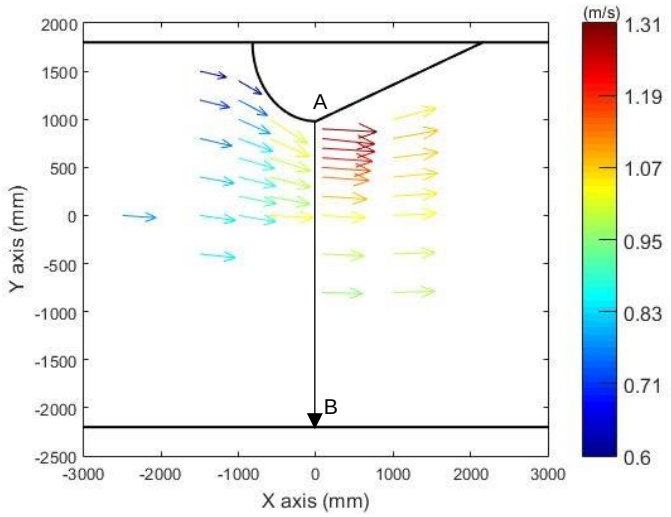

Figure 12. Vector plot from LDV data without turbine showing flow acceleration due to bluff body.

Figure 13 shows a comparison of the measured flow acceleration from the IFREMER flume tank test for the 1:20 scale model with those of the 1:40 scale tidal basin tests. The results are plotted for the line AB shown in Figure 12 with distance normalised with respect to bluff body diameter, D_b. Clearly, the 1:40 model show a significantly higher acceleration x/D_b, i.e. closer to the bluff body. This difference is attributed to friction effects associated with attachment of the 1:20 scale model to the concrete walls of the flume. This is investigated below using CFD.

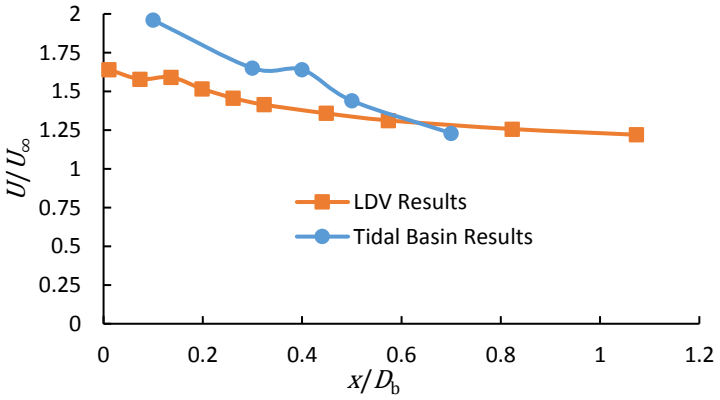

Figure 13. Comparison of measure flow acceleration versus distance from the bluff body for 1:20 IFREMER test and 1:40 tidal basin results.

To position the turbine and support its mass a hexapod was used, which was attached to an overhead gantry crane. Movement of the LDV required an additional gantry crane; this restricted flow measurement with the turbine in place to two transects downstream of the turbine. The resulting LDV data is shown in Figure 14, it is clear a turbulent wake forms behind the device. This discharge flow data is important for calibration of numerical and CFD models of the device in the future.

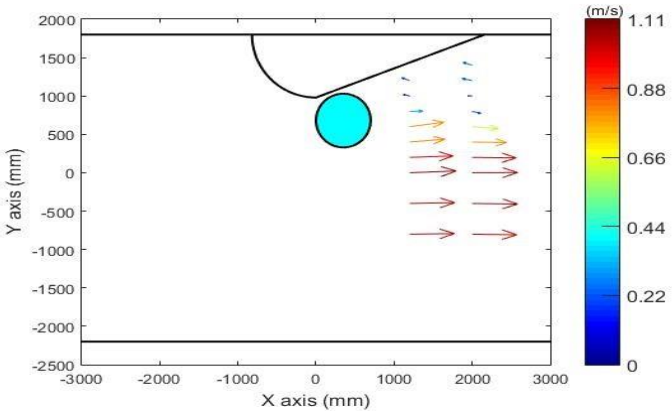

Figure 14.Vector plot of LDV data from 1:20 IFREMER flume tank tests with the turbine in position.

Following the testing protocols, the mechanical power is presented as C_P. A key aim of the 1:20 scale tank tests was to determine optimal turbine rotation speed for different free-stream flows. For each free-stream flow condition, a series of tests was conducted at different turbine rotation speeds. Each test was run for sufficient time to ensure steady state conditions. Figure 15 shows the C_P power curves for the tests. A peak C_P >30 % was achieved for all freestream flow speeds above 0.6 m/s. The peak C_P results for each test without the deflector are presented in Table 4, including the corresponding RPM and TSR values.

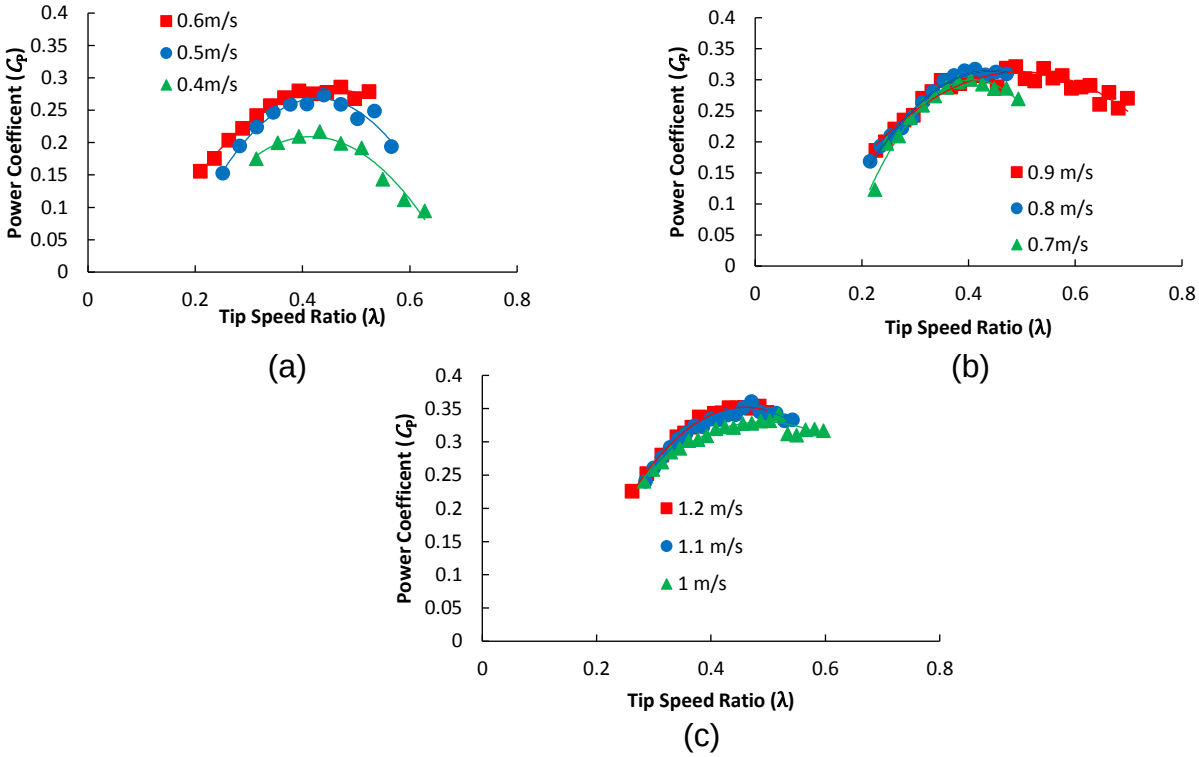

Figure 15. Full range of power curves for tests conducted with freestream velocities ranging from 0.4m/s to 1.2 m/s (a) 0.4 m/s to 0.6 m/s (b) 0.7 m/s to 0.9 m/s (c) 1 m/s to 1.2 m/s.

Table 4. Summary table of results for 1:20 scale model tests without the deflector.

Ambient Speed (m/s)	0.4	0.5	0.6	0.7	0.8	0.9	1.0	1.1	1.2
Max C_P	0.22	0.27	0.28	0.3	0.32	0.32	0.33	0.35	0.35
Optimum RPM	5	6.5	8.5	10	11.5	14.5	16	16	17.5
Optimum TSR	0.4	0.4	0.45	0.4	0.45	0.5	0.5	0.45	0.45

Based on some prior field observations, a small flow deflector was attached to the side bluff body immediately upstream of the turbine (see Figure 16). The flap has the effect of directing the accelerated flow onto the turbine blade as it begins to turn outward from the bluff body beginning its transition across the front end of the turbine. Figure 17 shows a comparison of the power curves for the 1:20 scale tests, at a flow speed of 1.1 m/s with and without the deflector. The effect of the flow deflector was to increase the peak C_P value from 0.35 to 0.4 and the corresponding TSR value from 0.5 to 0.55.

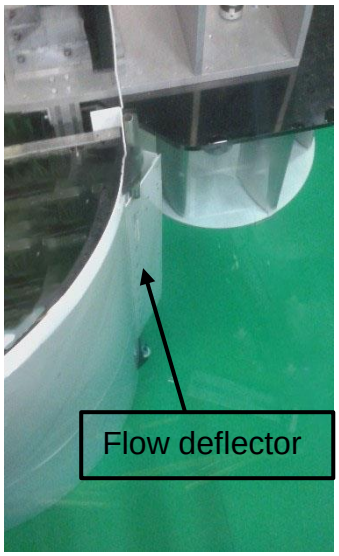

Figure 16. Image of flow deflector attached to bluff body.

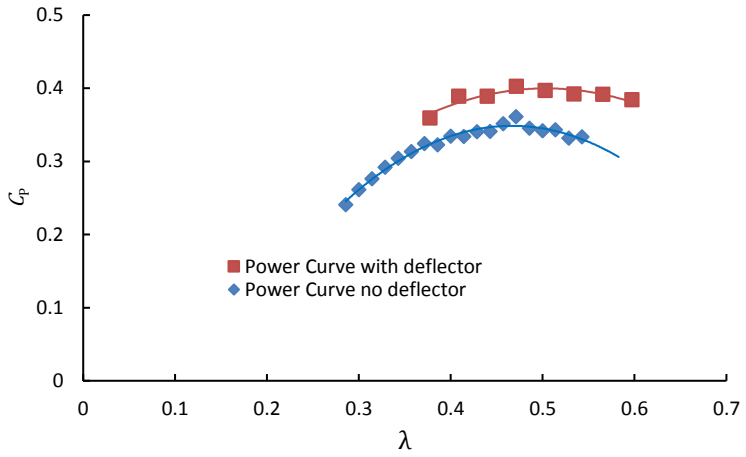

Figure 17. The measured effect of flow deflector on the power curve for 1:20 scale tests at 1.1 m/s flow speed. C_P versus TSR with/without the additional deflector.

Channel blockage (i.e. the ratio of the device frontal area to the channel cross-sectional area) is an important parameter in scale model testing of turbines. For the 1:20 scale tests, channel blockage $\varepsilon = 0.25$. Elevated blockage values can result in overestimation of C_P and testing protocols[23] recommend experimental results should be corrected to free stream conditions if $\varepsilon > 0.05$. While blockage correction methods have been developed for horizontal axis turbines, there are no accepted methods for vertical axis tidal turbines[14]. However, several attempts have been made, such as the works of Garrett and Cummins,[30] and extended by Whelan et al[31]. In this approach continuity and momentum conservation are utilised, by relating the free-stream velocity, wake velocity, device area and channel area to apply a correction. The by-pass velocity τ can be calculated as:

$$\tau = \frac{U_\infty - U_3 + \sqrt{[\varepsilon {U_\infty}^2 - 2\varepsilon U_\infty U_3 + (1 - \varepsilon + \varepsilon^2){U_3}^2]}}{1 - \varepsilon}$$

where U_3 is the downstream wake velocity. According to Whelan et al[31], both the torque and TSR should then be corrected to:

$$\left[\frac{C_T}{\tau^2}\right]_{(blocked)} = C_{T\,(unblocked)}$$

$$\left[\frac{\lambda}{\tau}\right]_{(blocked)} = \lambda_{(unblocked)}$$

In the present research, the wake by-pass velocity was calculated from measurements as 1.189 m/s for freestream velocity 1.1 m/s and a TSR of 0.45. Based on this, the peak performance coefficient determined at 1.1 m/s of 0.36 would be reduced to 0.25 and the TSR from 0.45 to 0.38. The validity of this approach for vertical axis turbines has been questioned by other studies[32] and is only presented here as an example of how correction might be applied. In the absence of an accepted method for correction for vertical axis turbines, performance results are left uncorrected.

Forces and moments on the turbine were sampled at a frequency of 100 Hz and averaged at one-minute intervals for each of the freestream velocities tested. The axial force was taken as the drag force. The data for just three flow velocities (for clarity)

are presented in Figure 18. Using this data and Equation 6, a C_D value of 0.75 was determined for the turbine.

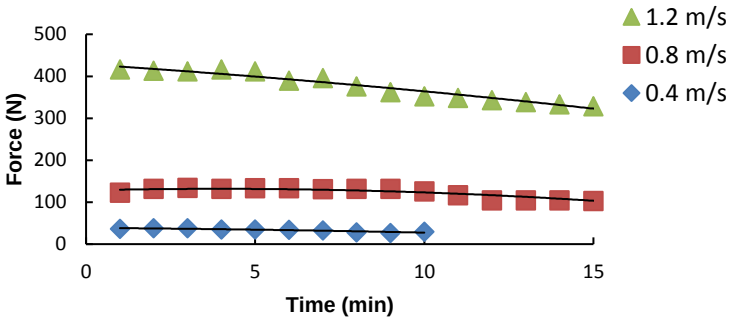

Figure 18. The turbine drag force with time histories.

The drag coefficient is dependent on the frontal profile of the structure and can vary from 0.4 for a curved profile to 1.4 for a flat plate. A turbine lies somewhere between these two profiles so the C_D value of 0.75 determined seems reasonable, particularly since this device has a high solidity (200 % when calculated using the ratio $\left[\frac{N_B C}{D}\right]$ where, N_B is the number of blades, C is the blade chord length and D is the turbine diameter.). This C_D value was then applied to omitted data (1 m/s) as a check to see how well it captured the drag loads in comparison to actual experimental data from the load cell. Figure 19 shows this comparison with a point for each free stream velocity tested; it can be seen that the theoretical values determined using the C_D value compare favourably with the experimental values.

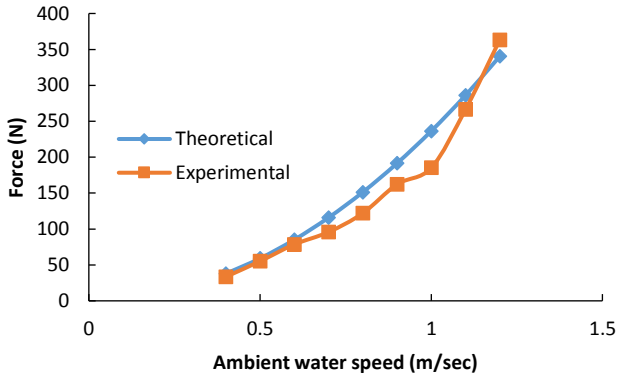

Figure 19. Theoretical versus experimental drag force on turbine from 0.4 m/s to 1.2 m/s.

3.3 CFD Model

CFD modelling was used to investigate the effect of the tank wall on the flow acceleration around the 1:20 scale model bluff body. Two models were created, one which included wall friction to induce a realistic boundary layer and the other with the boundary layer effect omitted, i.e. no friction.

From a mesh independent converged solution, three transects of data were taken from the model, corresponding to those from the experimental LDV data. A schematic for the location of these transects is presented in Figure 20. A comparison of CFD data

vs LDV measured data for the three transects is presented in Figure 21. It is clear that there is general agreement between the CFD and the LDV experimental data. Presented in Figure 22 is a vector plot from the CFD model. The area of highest acceleration can be observed at the widest point of the bluff body.

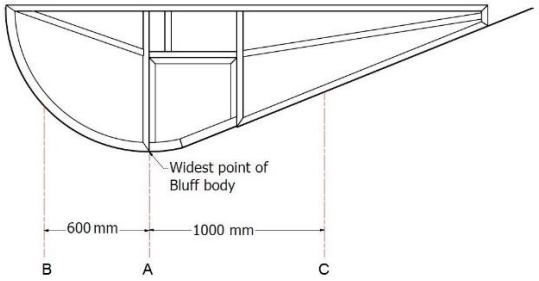

Figure 20. Schematic for the location of the three data transects, A,B and C, located at the widest part of the bluff body, 600 mm in front and 1 m behind respectively.

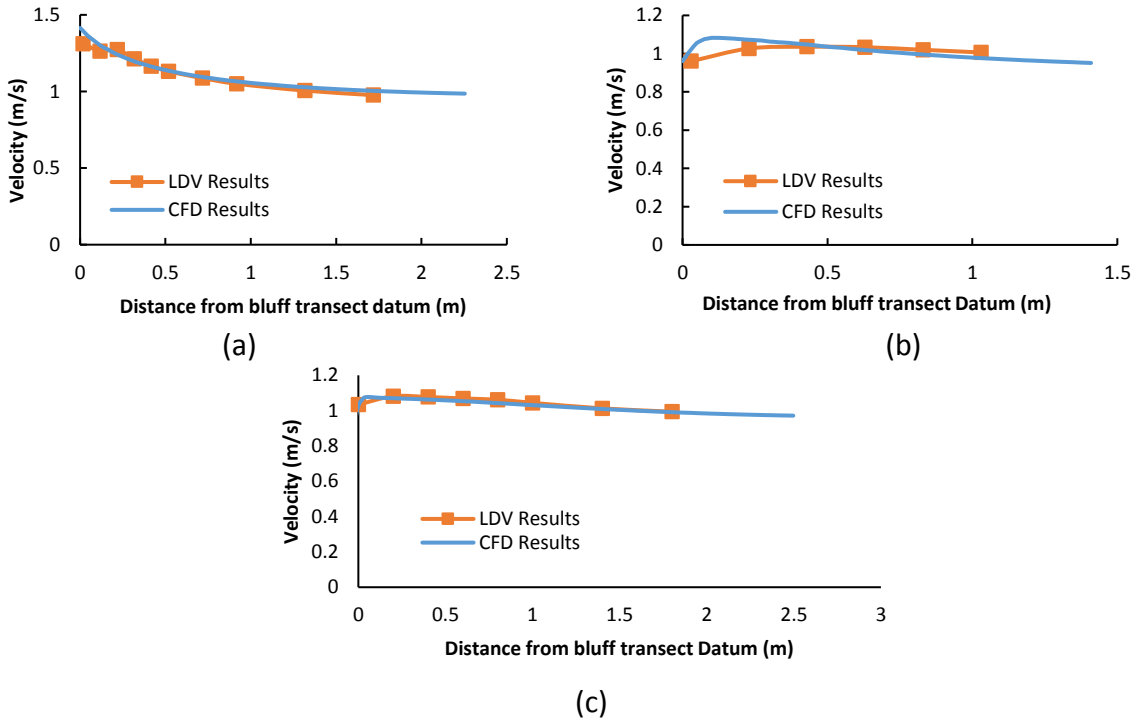

Figure 21. Comparison of CFD data vs LDV measured data for the three transects. (a), (b) and (c) with corresponding transects A, B and C.

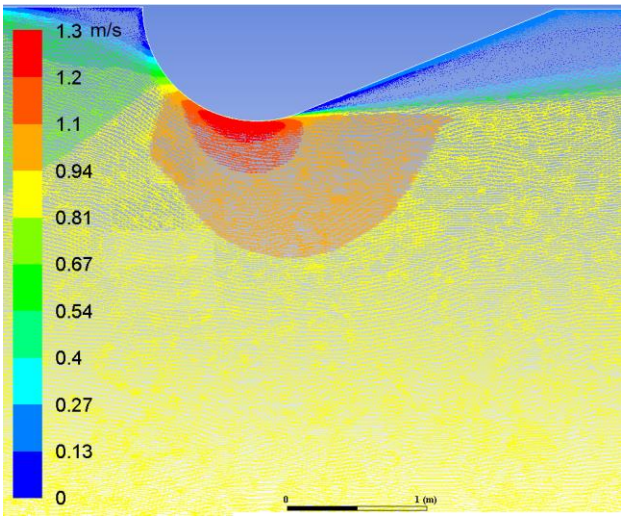

Figure 22. CFD Vector plot with included boundary layer effect at the walls.

A CFD vector plot from the model without wall friction, is presented in Figure 23. The highest acceleration above the ambient of 0.8 m/s occurs at the widest part of the bluff body; a velocity of 1.6 m/s can be observed at this location, corresponding to an increase by a factor of 2.

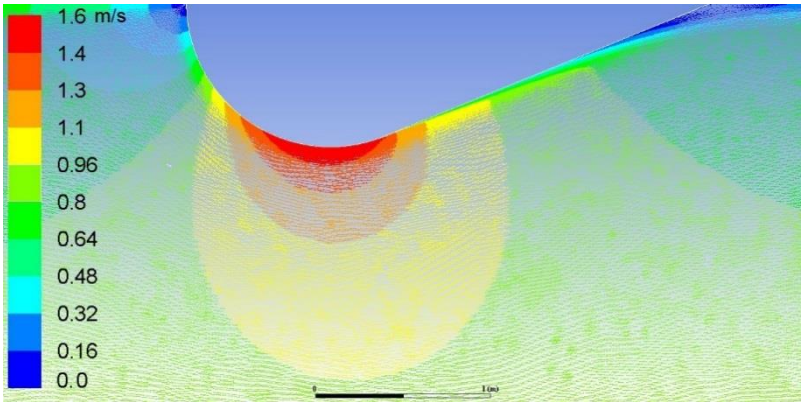

Figure 23. CFD vector plot without boundary layer effect at the walls.

Figure 24 compares the localised accelerations to the tidal basin accelerations along Transect A in Figure 18. It can be seen that there is significantly better agreement with the tidal basin data than in Figure 12. This confirms that the reduced accelerations measured in the 1:20 scale tests can indeed be attributed to the wall friction-induced boundary layer.

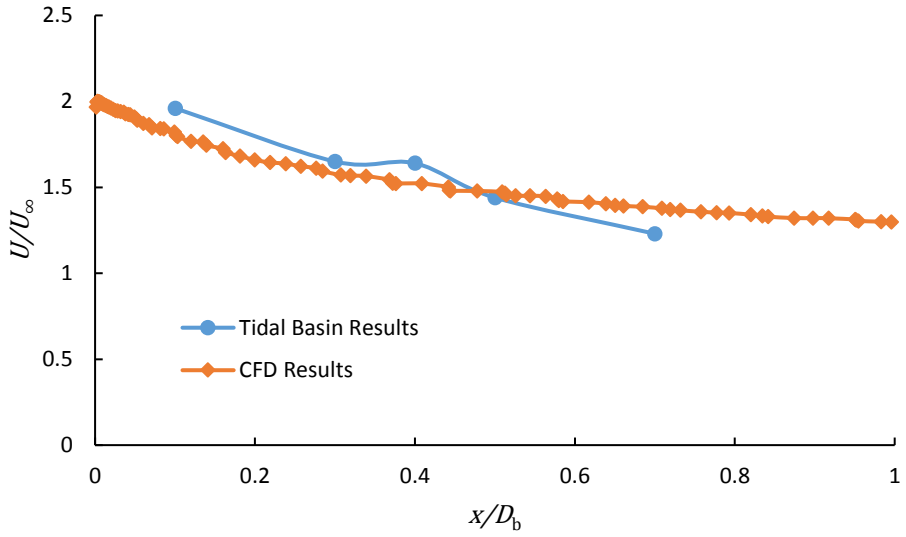

Figure 24. Comparison of CFD model data versus Tidal basin measured results.

4 Discussion

Testing of a 1:40 scale model of the bluff body in a tidal basin showed that the bluff body is capable of accelerating the freestream flow by a factor of 2. This is comparable to the levels of localised flow acceleration observed in previous studies of flow around cylinders, e.g. Graf and Yulistiyanto[10] recorded accelerations of 100 % in depth-averaged flow speeds around a submerged cylinder. The LDV flow measurements for the 1:20 scale model of the bluff body confirmed its flow-accelerating potential. Although the levels of acceleration were not as high (approximately a factor of 1.6) the accelerated inlet flows led to high mechanical efficiencies in the region of 35 to 40 %. CFD analyses provided the connection between the two sets of experimental flow data and proved that the lower accelerations in the 1:20 scale tests were the result of the boundary layer formed due to the friction effect of the tank wall. The CFD results with the wall friction included gave good agreement with the measured data and when the wall friction was removed the modelled accelerations increased to levels similar to those recorded in the 1:40 tidal basin tests. The LDV was used to measure flow-fields around the device with the turbine in-situ from which the effects of the turbine are easily apparent in the turbine wake. These measured datasets will be for validation of future CFD models of the device.

The drag loads recorded on the full 1:40 scale device made it possible to determine a drag coefficient of 0.68 for the complete device (bluff body and two turbines). Knowledge of the drag coefficient will prove beneficial for upscaling of the device and determination of mooring loads for field tests. The 1:20 scale test determine a drag coefficient of 0.75 for the turbine alone.

The method developed for measuring mechanical power, where a torque meter was built using strain gauges and a data logger, is much less invasive than the more commonly used torque transducer which involves splitting the turbine shaft and additional couplings. The approach worked very well here and yielded accurate results. It may prove useful in other scale model turbine studies where a non-invasive technique is desirable.

The performance results from the 1:20 scale model show that the device is a viable design, with a peak efficiency of 35 % achieved at a freestream flow speed of 1.1 m/s. By attaching a small flow deflector to the bluff body immediately upstream of the turbine entrance, the peak efficiency was improved to 40 % for the same flow speed. By way of comparison to other devices of similar design, New Energy Corporation[15] achieved an efficiency of 32 % for their fixed-pitch vertical axis turbine, and Jing et al[16] achieved 25 % for their variable-pitch design. The better performance of the device presented here is ascribed to the flow acceleration and the variable pitch blades. Without test results of a similar device with fixed pitch blades, it is difficult to determine which of the two design features most greatly influences performance but the authors are currently developing a CFD model of the device which will be used to answer this question.

As mentioned previously, some ducted turbine studies[19-20] incorrectly use the smaller turbine area, rather than the larger duct area to calculate C_P. This has the effect of computing much higher C_P values. For the sake of comparison, if the reference area for C_P calculations of the device presented here was taken as the smaller turbine entrance area rather than the full device entrance area, the peak C_P value for the device would increase from 0.4 to 0.95. This compares very well with the values quoted for ducted turbines (range of 0.3 to 0.45)[19,20].

5 Conclusions

A novel vertical axis turbine including flow acceleration and variable pitch blades has been tested at 1:40 scale and 1:20 scale. The following are the main conclusions from the research:

- Use of the bluff body acts to accelerate the inlet flows to the turbines. Without the turbines present, the bluff body is capable of accelerating the free-stream flow by a factor of 2.
- The peak mechanical efficiency of 40 % is higher than many other vertical axis turbines for which results are available. It is acknowledged, however, that the measured efficiencies may contain some inaccuracy due to the high channel blockage of the 1:20 scale tests. Unfortunately, there is currently no accepted method for blockage correction of vertical axis turbine test results. Even so, the recorded efficiencies are such that the device, therefore, merits further research and development.
- There are a limited number of locations worldwide with the peak flow speeds in excess of 2 m/s, that are generally quoted as the requirement for tidal turbines to operate economically. By accelerating the free-stream flows, the present device can operate in less energetic tidal, or indeed river currents.
- The initial CFD model presented here is currently being used to develop a much more complex CFD model of the full device (including turbines and bluff body) using sliding meshes to model the variable pitch blades. The model will enable design changes to be evaluated without the expense of experimental testing. In this respect, the measured datasets presented here are a hugely important resource for model validation.

Acknowledgements
This material is based upon works supported by Science Foundation Ireland under Grant No. 12/RC/2302 through MaREI, the national centre for Marine and Renewable Energy Ireland and by Sustainable Energy Authority of Ireland through their Prototype Development Fund.
The authors wish to acknowledge the DJEI/DES/SFI/HEA Irish Centre for High-End Computing (ICHEC) for the provision of computational facilities and support.

References

1. Rolland SA, Thatcher M, Newton W, et al. Benchmark experiments for simulations of a vertical axis wind turbine. *Applied Energy* 2013; 111: 1183–1194.
2. Fraenkel P. Practical tidal turbine design considerations : a review of technical alternatives and key design decisions leading to the development of the SeaGen 1 . 2MW tidal turbine. *Ocean Power Fluid Machinery Seminar* 2010; 1–19.
3. Ladokun LL, Ajao KR, Sule BF. Hydrokinetic Energy Conversion Systems : Prospects and Challenges in Nigerian Hydrological Setting. *Nigerian Journal of Technology* 2013; 32: 538–549.
4. Andritz Hydro Hammerfest. ANDRITZ HYDRO Hammerfesthttp://www.andritzhydrohammerfest.co.uk/references/ (accessed 1 February 2017).
5. Rajgor G. Tidal developments power forward. *Renewable Energy Focus* 2016; 17: 147–149.
6. Zhou Z, Benbouzid M, Charpentier J-F, et al. Developments in large marine current turbine technologies – A review. *Renewable and Sustainable Energy Reviews* 2017; 71: 852–858.
7. Laws ND, Epps BP. Hydrokinetic energy conversion: Technology, research, and outlook. *Renewable and Sustainable Energy Reviews* 2016; 57: 1245–1259.
8. Roddier D, Cermelli C, Aubault A. Electrical Power Generation by Tidal Flow Acceleration. In: *26th International Conference on Offshore Mechanics and Arctic Engineering OMAE2007*. 2007, pp. 1–6.
9. Gerrard JH. The mechanics of the formation region of vortices behind bluff bodies. *Journal of Fluid Mechanics* 1966; 25: 401.
10. Graf WH, Yulistiyanto B. Experiments on flow around a cylinder; the velocity and vorticity fields. *Journal of Hydraulic Research* 1998; 36: 637–653.
11. O'Doherty T, Mason-Jones a., O'Doherty DM, et al. Experimental and Computational Analysis of a Model Horizontal Axis Tidal Turbine. *Proceedings of the 8th European Wave and Tidal Energy Conference* 2009; 833–841.
12. Clarke JA, Connor G, Grant AD, et al. Design and testing of a contra-rotating tidal current turbine. *Journal of Power and Energy* 2007; 221: 171–179.
13. Goundar JN, Ahmed MR. Design of a horizontal axis tidal current turbine. *Applied Energy* 2013; 111: 161–174.
14. Bachant P, Wosnik M. Effects of reynolds number on the energy conversion and near-wake dynamics of a high solidity vertical-axis cross-flow turbine. *Energies* 2016; 9(2): 73.
15. New Energy Corporation. EnCurrent Hydro Turbines 5 and 10 kW Specifications. 2015; 1–2.
16. Jing F, Sheng Q, Zhang L. Experimental research on tidal current vertical axis

turbine with variable-pitch blades. *Ocean Engineering* 2014; 88: 228–241.
17. Birjandi AH, Bibeau EL, Chatoorgoon V, et al. Power measurement of hydrokinetic turbines with free-surface and blockage effect. *Ocean Engineering* 2013; 69: 9–17.
18. Li Y. On the definition of the power coefficient of tidal current turbines and efficiency of tidal current turbine farms. *Renewable Energy* 2014; 68: 868–875.
19. Elbatran AH, Ahmed YM, Shehata AS. Performance study of ducted nozzle Savonius water turbine, comparison with conventional Savonius turbine. *Energy* 2017; 134: 566–584.
20. Derakhshan S, Ashoori M, Salemi A. Experimental and numerical study of a vertical axis tidal turbine performance. *Ocean Engineering* 2017; 137: 59–67.
21. Jin X, Wang Y, Ju W, et al. Investigation into parameter in fl uence of upstream de fl ector on vertical axis wind turbines output power via three-dimensional CFD simulation. *Renewable Energy* 2018; 115: 41–53.
22. McCombes T, Johnstone CM, Holmes B, et al. Best practice for tank testing of small marine energy devices. *EquiMar Project* 2010; 1–48.
23. Bahaj AS, Blunden L, Anwar and AA. University of Southampton. OES IA Annex II Task 2.2 Tidal Energy Development Protocol, Report from BERR for the OES-IA.www.iea-oceans.org (2008).
24. Dane HJ. Ultrasonic measurement of unsteady gas flow. *Flow Measurement and Instrumentation* 1998; 8: 183–190.
25. Sumer BM, Fredsoe J. *Hydrodynamics Around Cylindricalstructures*. 2006. Epub ahead of print 2006. DOI: 10.1016/S0378-3839(97)00031-8.
26. Menter FR. Zonal Two Equation k-w, Turbulence Models for Aerodynamic Flows. *AIAA paper* 1993; 2906.
27. Menter FR, Langtry R, Völker S, et al. Transition Modelling for General Purpose CFD Codes. *Engineering Turbulence Modelling and Experiments 6* 2005; 31–48.
28. Menter FR. 2-Equation eddy-visocity turbulence models for engineering applications. *Aiaa Journal* 1994; 32: 1598–1605.
29. Zhang K, Katsuchi H, Zhou D, et al. Numerical study on the effect of shape modification to the flow around circular cylinders. *Journal of Wind Engineering and Industrial Aerodynamics* 2016; 152: 23–40.
30. GARRETT C, CUMMINS P. The efficiency of a turbine in a tidal channel. *Journal of Fluid Mechanics* 2007; 588: 243–251.
31. WHELAN JI, GRAHAM JMR, PEIRÓ J. A free-surface and blockage correction for tidal turbines. *Journal of Fluid Mechanics* 2009; 624: 281.
32. Robert Cavagnaro BP. An Evaluation of Blockage Corrections for a Helical Cross-Flow Turbine. In: *3rd Oxford Tidal Energy Workshop*. 2014. Epub ahead of print 2014. DOI: 10.2514/1.44602.